

Support information

Screening thermoelectric materials for high output performance in wearable electronics

Xinjie Yuan^{a,b}, Pengfei Qiu^{*a,b,c}, Chuanyao Sun^{a,b}, Shiqi Yang^a, Yi Wu^{a,b}, Yumeng Wang^{a,b}, Ming Gu^a, Lidong Chen^{a,b}, Xun Shi^{*a,b}

^a State Key Laboratory of High Performance Ceramics and Superfine Microstructure, Shanghai Institute of Ceramics, Chinese Academy of Sciences, Shanghai 200050, China.

^b Center of Materials Science and Optoelectronics Engineering, University of Chinese Academy of Sciences, Beijing 100049, China

^c School of Chemistry and Materials Science, Hangzhou Institute for Advanced Study, University of Chinese Academy of Sciences, Hangzhou 310024, China

*Corresponding authors.

E-mails: qiupf@mail.sic.ac.cn, xshi@mail.sic.ac.cn.

Supporting Text

One-dimensional heat transfer model

Here the simplified one-dimensional heat transfer model was used to derive the maximum voltage density (V_{OC}/A) and power density (P_{max}/A) of a TE leg with the cold end surface directly exposed to air (**Fig. S1**). The one-dimensional model is derived under the following assumptions. 1) The model contains only one homogenous TE leg. 2) The heat flow inside the TE leg is unidirectional from heat source to air. 3) The four side surfaces of the TE leg are assumed to be adiabatic and only the heat in the upper surface is convectively exchanged with air. 4) The physical properties of the TE leg are temperature independent. 5) Contact electric/thermal resistance at the interface between TE leg and heat source is set zero. Under these assumptions, the thermal resistance of the TE leg (θ_{leg}), the thermal resistance between the air and TE leg (θ_{air}), and the temperature difference on the TE leg (ΔT_{leg}) can be expressed as

$$\theta_{leg} = \frac{l}{\kappa A} \quad (1)$$

$$\theta_{air} = \frac{1}{h_{air}A} \quad (2)$$

$$\Delta T_{leg} = \frac{T_h - T_{air}}{\theta_{leg} + \theta_{air}} \theta_{leg} \quad (3)$$

Substituting Equations (1) and (2) into Equation (3) yields

$$\Delta T_{leg} = \frac{h_{air}l}{h_{air}l + \kappa} (T_h - T_{air}) \quad (4)$$

The open circuit voltage (V_{OC}) of the TE leg can be described as

$$V_{OC} = |S| \Delta T_{leg} \quad (5)$$

Substituting Equation (4) into Equation (5) yields

$$V_{OC} = \frac{|S|h_{air}l}{h_{air}l + \kappa} (T_h - T_{air}) \quad (6)$$

The internal resistance (R_{in}) and maximum output power (P_{max}) of the TE leg are described as

$$R_{in} = \frac{l}{\sigma A} \quad (7)$$

$$P_{max} = \frac{V_{OC}^2}{4R_{in}} \quad (8)$$

Substituting Equations (6) and (7) into Equation (8) yields

$$P_{max} = \frac{S^2 \sigma}{(h_{air}l + \kappa)^2} \frac{(T_h - T_{air})^2 h_{air}^2 l A}{4} \quad (9)$$

The voltage density (V_{OC}/A) and power density (P_{max}/A) of the TE leg can be expressed as

$$V_{OC} / A = \frac{|S|h_{air}l}{A(h_{air}l + \kappa)} (T_h - T_{air}) \quad (10)$$

$$P_{max} / A = \frac{S^2 \sigma}{(h_{air}l + \kappa)^2} \frac{(T_h - T_{air})^2 h_{air}^2 l}{4} \quad (11)$$

where S is the Seebeck coefficient, σ is the electrical conductivity, κ is the thermal conductivity, l is the height of the TE leg, A is the cross-sectional area of the TE leg, h_{air} is the heat transfer coefficient, T_h is the temperature of the heat source, and T_{air} is the ambient temperature.

It should be noted that there are many limitations for this one-dimensional model. For example, in the real case, the TE leg includes the solder, metallization layer, and electrode. The electric/thermal resistance at the interfaces cannot be neglected. In addition, the heat flow inside

the TE leg is not unidirectional, and the heat would be also dissipated from the four side surfaces of the TE leg. Thus, this simplified model can just qualitatively give the main influence factors to V_{OC}/A and P_{max}/A .

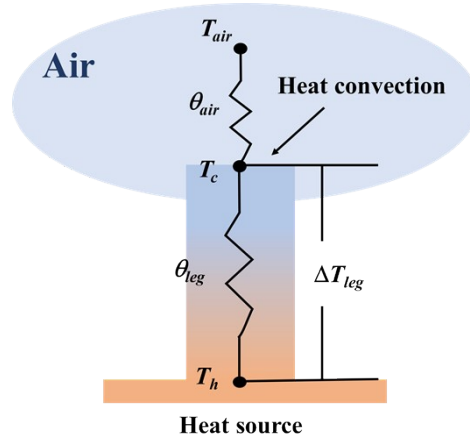


Fig. S1 Schematics for the simplified one-dimensional heat transfer model used for the derivation of maximum voltage density (V_{OC}/A) and power density (P_{max}/A).

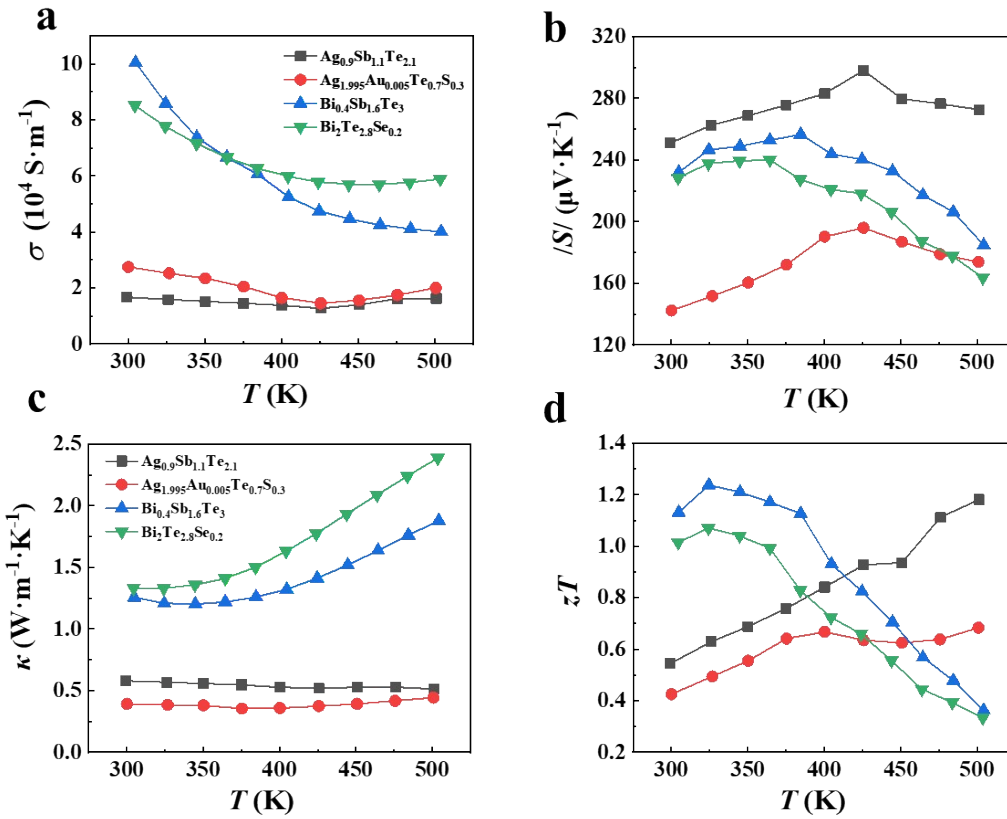


Fig. S2 TE properties of $\text{Ag}_{1.995}\text{Au}_{0.005}\text{Te}_{0.7}\text{S}_{0.3}$, $\text{Ag}_{0.9}\text{Sb}_{1.1}\text{Te}_{2.1}$, $\text{Bi}_{0.4}\text{Sb}_{1.6}\text{Te}_3$, and $\text{Bi}_2\text{Te}_{2.8}\text{Se}_{0.2}$. (a) Temperature dependences of electrical conductivity σ , (b) absolute value of Seebeck coefficient $|S|$, (c) thermal conductivity κ , and d) TE figure-of-merit zT .

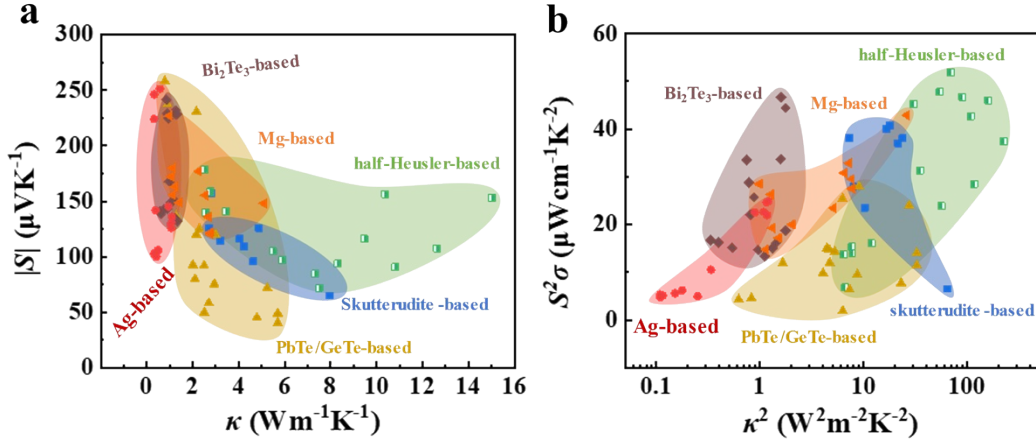


Fig. S3 Room-temperature performance of typical TE materials. (a) $|S|$ vs κ and (b) $S^2\sigma$ vs κ^2 . The data are taken from Ref. 41.¹

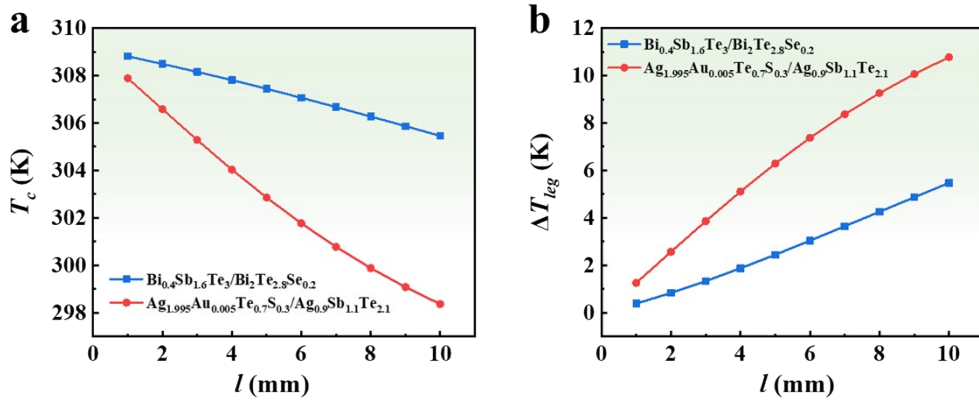


Fig. S4 Simulated (a) cold side temperature (T_c) and (b) temperature difference (ΔT_{leg}) across the TE legs as a function of the length of the TE leg (l) for the $\text{Ag}_{1.995}\text{Au}_{0.005}\text{Te}_{0.7}\text{S}_{0.3}/\text{Ag}_{0.9}\text{Sb}_{1.1}\text{Te}_{2.1}$ TE device. The data of $\text{Bi}_{0.4}\text{Sb}_{1.6}\text{Te}_3/\text{Bi}_2\text{Te}_{2.8}\text{Se}_{0.2}$ TE device are included for comparison.

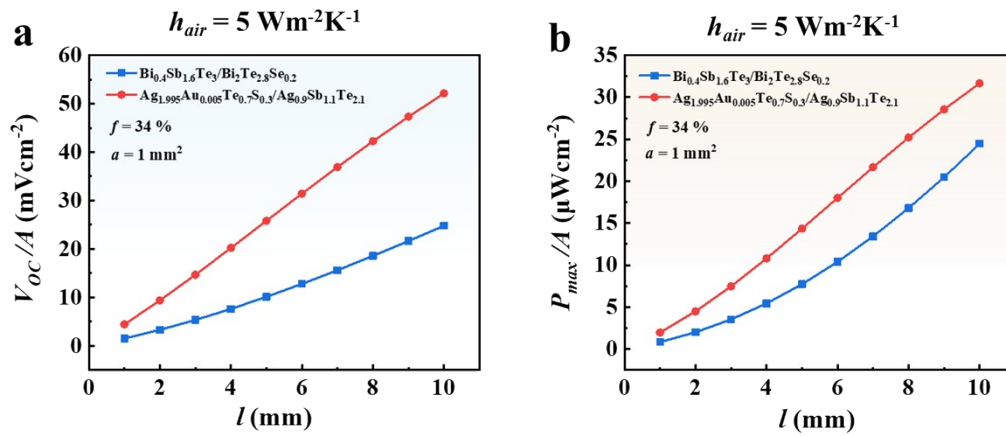


Fig. S5 Simulated (a) voltage density (V_{OC}/A) and (b) power density (P_{max}/A) as a function of TE leg's height (l) for the $\text{Ag}_{1.995}\text{Au}_{0.005}\text{Te}_{0.7}\text{S}_{0.3}/\text{Ag}_{0.9}\text{Sb}_{1.1}\text{Te}_{2.1}$ TE device and $\text{Bi}_{0.4}\text{Sb}_{1.6}\text{Te}_3/\text{Bi}_2\text{Te}_{2.8}\text{Se}_{0.2}$ TE device under the heat transfer coefficient (h_{air}) of $5 \text{ Wm}^{-2}\text{K}^{-1}$.

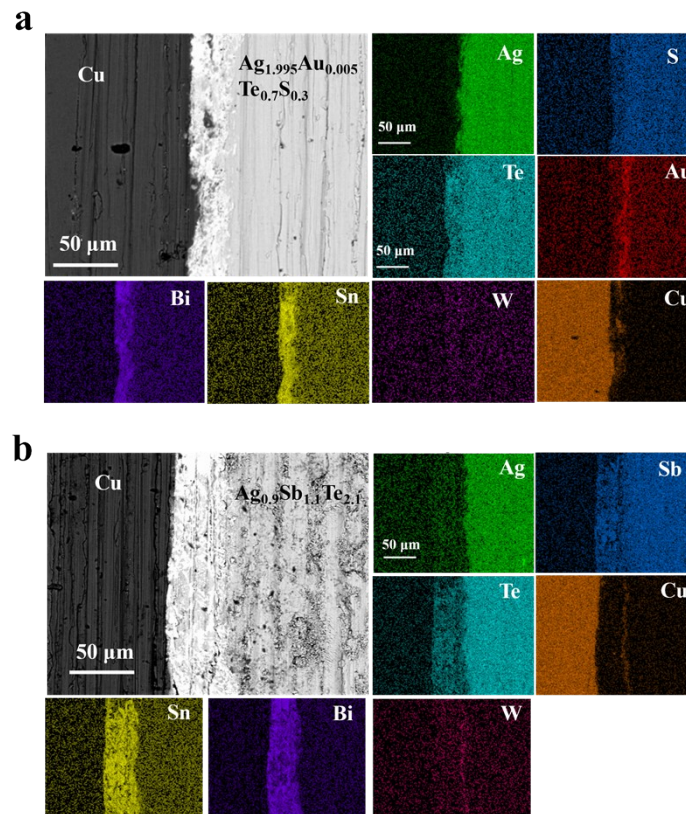


Fig. S6 Backscattered electron image and elemental energy dispersive spectroscopy (EDS) mappings at the (a) $\text{Ag}_{1.995}\text{Au}_{0.005}\text{Te}_{0.7}\text{S}_{0.3}/\text{W}/\text{Sn}/\text{Cu}$ interface and (b) $\text{Ag}_{0.9}\text{Sb}_{1.1}\text{Te}_{2.1}/\text{W}/\text{Sn}/\text{Cu}$ interface.

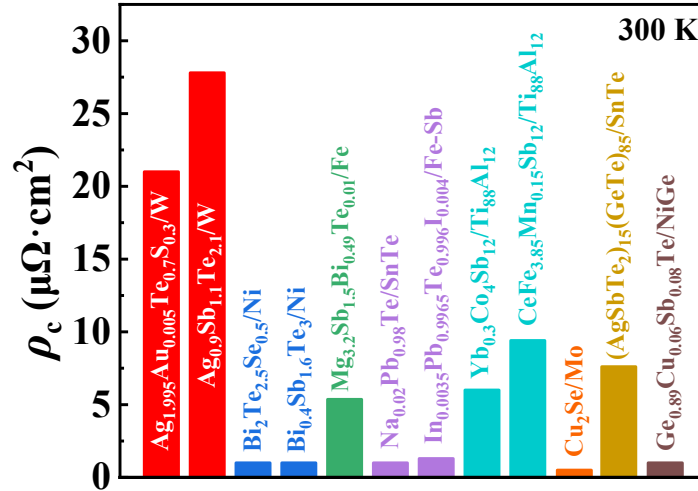


Fig. S7 Comparison on the contact electrical resistivity (ρ_c) of the $\text{Ag}_{1.995}\text{Au}_{0.005}\text{Te}_{0.7}\text{S}_{0.3}/\text{W}$ and $\text{Ag}_{0.9}\text{Sb}_{1.1}\text{Te}_{2.1}/\text{W}$ interfaces with those reported for the state-of-the-art TE materials.²⁻⁸

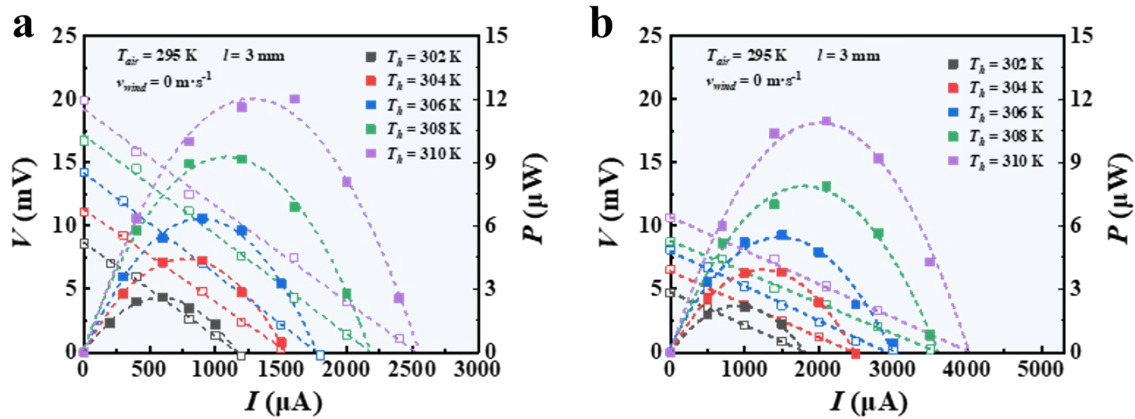


Fig. S8 Measured output voltage (V) and output power (P) as a function of current (I) under different hot side temperatures (T_h) for (a) $\text{Ag}_{1.995}\text{Au}_{0.005}\text{Te}_{0.7}\text{S}_{0.3}/\text{Ag}_{0.9}\text{Sb}_{1.1}\text{Te}_{2.1}$ TE device and (b) $\text{Bi}_{0.4}\text{Sb}_{1.6}\text{Te}_3/\text{Bi}_2\text{Te}_{2.8}\text{Se}_{0.2}$ TE device. The ambient temperature (T_{air}) is 295 K.

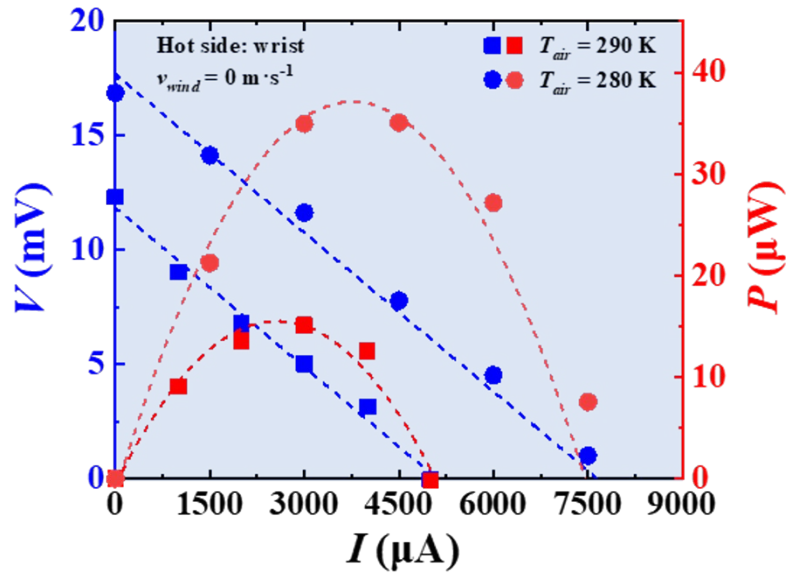


Fig. S9 Measured voltage (V) and power output (P) as a function of current (I) when the $\text{Bi}_{0.4}\text{Sb}_{1.6}\text{Te}_3/\text{Bi}_2\text{Te}_{2.8}\text{Se}_{0.2}$ TE device is worn on the human wrist. The ambient temperature is 290 K and 280 K, respectively.

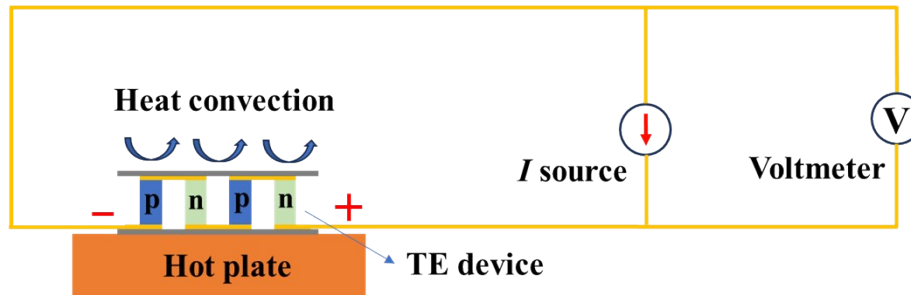


Fig. S10 Schematics of the home-made TE device test platform. The device is placed on a hot plate. The upper end of the device exchanges heat with the environment in a way of natural heat convection.

Table S1. Comparison on the output performance (V_{OC}/A and P_{max}/A) of the $\text{Ag}_{1.995}\text{Au}_{0.005}\text{Te}_{0.7}\text{S}_{0.3}/\text{Ag}_{0.9}\text{Sb}_{1.1}\text{Te}_{2.1}$ TE device prepared in this work and the Bi_2Te_3 -based TE devices reported before. All data are taken from the wearing condition when the devices are worn on human body in the windless indoor environment without additional cooling facilities.^{9–15} The

device parameters, including the cross-sectional area (A) and the length of TE legs (l), and the ambient temperature during the measurement (T_{air}) are included for each TE device.

Composition	A (cm ²)	V_{oc}/A (mVcm ⁻²)	P_{max}/A (μ Wcm ⁻²)	T_{air} (K)	l (mm)
Bi ₂ Se _{0.3} Te _{2.7} /Bi _{0.5} Sb _{1.5} Te ₃	300.0	0.48	1.42	297	5
Bi ₂ Se _{0.3} Te _{2.7} /Bi _{0.5} Sb _{1.5} Te ₃	25.0	2.98	4.50	295	5
Bi ₂ Se _{0.3} Te _{2.7} /Bi _{0.5} Sb _{1.5} Te ₃	25.0	4.68	10.70	283	5
Bi ₂ Se _{0.3} Te _{2.7} /Bi _{0.5} Sb _{1.5} Te ₃	16.8	15.86	6.96	~290	2
Bi ₂ Se _{0.3} Te _{2.7} /Bi _{0.5} Sb _{1.5} Te ₃	16.5	1.33	5.98	291	3.7
Bi _{1.991} Ag _{0.009} Te _{2.691} Se _{0.3} I _{0.009} /Bi _{0.4} Sb _{1.6} Te ₃	2.3	14.21	7.89	287	3.14
Bi _{0.8} Sb _{1.2} Te ₃ /Ag ₂ Se _{0.67} S _{0.33}	6.5	0.92	0.40	293	0.1
Bi ₂ Te ₃ /Bi _{0.4} Sb _{1.6} Te ₃	20.3	0.68	0.14	~290	6
Ag _{1.995} Au _{0.005} Te _{0.7} S _{0.3} /Ag _{0.9} Sb _{1.1} Te _{2.1}	1.0	22.72	20.55	290	3
Ag _{1.995} Au _{0.005} Te _{0.7} S _{0.3} /Ag _{0.9} Sb _{1.1} Te _{2.1}	1.0	32.59	42.03	280	3

Table S2 Rom-temperature TE properties and physical properties of Ag_{0.9}Sb_{1.1}Te_{2.1}, Ag_{1.995}Au_{0.005}Te_{0.7}S_{0.3}, Bi_{0.4}Sb_{1.6}Te₃, and Bi₂Te_{2.8}Se_{0.2} used for the simulation.

	σ (S·m ⁻¹)	κ (W·m ⁻¹ ·K ⁻¹)	S (μ V·K ⁻¹)	ρ (kg·m ⁻³)	C_p (J·kg ⁻¹ ·K ⁻¹)
Ag _{0.9} Sb _{1.1} Te _{2.1}	18000	0.58	247	6592	205
Ag _{1.995} Au _{0.005} Te _{0.7} S _{0.3}	28000	0.39	-139	7460	238
Bi _{0.4} Sb _{1.6} Te ₃	100450	1.26	232	6737	186
Bi ₂ Te _{2.8} Se _{0.2}	85000	1.33	-228	7584	162

Reference

- 1 G. S. Na and H. Chang, *npj Comput. Mater.*, 2022, **8**, 214.
- 2 A. Singh, S. Bhattacharya, C. Thinaharan, D. K. Aswal, S. K. Gupta, J. V. Yakhmi and K. Bhanumurthy, *J. Phys. D: Appl. Phys.*, 2008, **42**, 015502.
- 3 P. Qiu, T. Mao, Z. Huang, X. Xia, J. Liao, M. T. Agne, M. Gu, Q. Zhang, D. Ren, S. Bai, X. Shi, G. J. Snyder and L. Chen, *Joule*, 2019, **3**, 1538–1548.
- 4 L. Xie, C. Ming, Q. Song, C. Wang, J. Liao, L. Wang, C. Zhu, F. Xu, Y.-Y. Sun, S. Bai and L. Chen, *Sci. Adv.*, 2023, **9**, eadg7919.
- 5 L. Yin, F. Yang, X. Bao, W. Xue, Z. Du, X. Wang, J. Cheng, H. Ji, J. Sui, X. Liu, Y. Wang, F. Cao, J. Mao, M. Li, Z. Ren and Q. Zhang, *Nat. Energy*, 2023, **8**, 665–674.
- 6 G. Joshi, D. Mitchell, J. Ruedin, K. Hoover, R. Guzman, M. McAleer, L. Wood and S. Savoy, *J. Mater. Chem. C*, 2019, **7**, 479–483.
- 7 Q. Zhang, J. Liao, Y. Tang, M. Gu, C. Ming, P. Qiu, S. Bai, X. Shi, C. Uher and L. Chen, *Energy Environ. Sci.*, 2017, **10**, 956–963.
- 8 L. Yin, C. Chen, F. Zhang, X. Li, F. Bai, Z. Zhang, X. Wang, J. Mao, F. Cao, X. Chen, J. Sui, X. Liu and Q. Zhang, *Acta Mater.*, 2020, **198**, 25–34.
- 9 S. Khan, J. Kim, K. Roh, G. Park, and W. Kim, *Nano Energy*, 2021, **87**, 106180.
- 10 B. Lee, H. Cho, K. T. Park, J.-S. Kim, M. Park, H. Kim, Y. Hong, and S. Chung, *Nat. Commun.*, 2020, **11**, 5948.
- 11 W. Fan, Z. Shen, Q. Zhang, F. Liu, C. Fu, T. Zhu, and X. Zhao, *ACS Appl. Mater. Interfaces*, 2022, **14**, 21224–21231.
- 12 W. Chen, X.-L. Shi, M. Li, T. Liu, Y. Mao, Q. Liu, M. Dargusch, J. Zou, G. Q. Lu and Z.-G. Chen, *Science*, 2024, **386**, 1265–1271.
- 13 T. Deng, Z. Gao, Z. Li, P. Qiu, Z. Li, X. Yuan, C. Ming, T.-R. Wei, L. Chen and X. Shi, *Science*, 2024, **386**, 1112–1117.
- 14 Y. Jing, J. Luo, X. Han, J. Yang, Q. Liu, Y. Zheng, X. Chen, F. Huang, J. Chen, Q. Zhuang, Y. Shen, H. Chen, H. Zhao, G. J. Snyder, G. Li, T. Zhang and K. Zhang, *Energy Environ. Sci.*, 2023, **16**, 4334–4344.
- 15 S. Hong, Y. Gu, J. K. Seo, J. Wang, P. Liu, Y. S. Meng, S. Xu and R. Chen, *Sci. Adv.*, 2019, **5**, eaaw0536.